RSC Advances

PAPER

View Article Online
View Journal | View Issue

Cite this: *RSC Adv.*, 2023, **13**, 29121

A copper(II) complex containing pyridine-2-carbaldehyde and its direct binding onto ethylenediamine functionalized with Fe_3O_4@SiO_2 nanoparticles for catalytic applications†

Masoud Karimi,[a] Ali Ramazani, *[ab] Sami Sajjadifar [c] and Sobhan Rezayati [a]

In the present study, a copper(II) complex containing a pyridine-2-carbaldehyde ligand and its direct binding onto ethylenediamine functionalized with Fe_3O_4@SiO_2 nanoparticles [Cu(II)-Schiff base-$(CH_2)_3$-SiO_2@Fe_3O_4] as a heterogeneous magnetic nanocatalyst can be easily prepared using a multi-step method. Next, the structural and magnetic properties of the synthesized nanoparticles were identified using Fourier-transform infrared spectroscopy (FT-IR), inductively coupled plasma (ICP), vibrating-sample magnetometry (VSM), transmission electron microscopy (TEM), field-emission scanning electron microscopy (FE-SEM), thermogravimetric analysis (TGA), PXRD (Powder X-ray diffraction), Brunauer–Emmett–Teller (BET), and energy-dispersive X-ray spectrometry (EDX) techniques. TEM images reveal that the average particle size distribution was found to be in the range of 45–55 nm with spherical shape. The PXRD analysis indicated that the crystallite size was found to be 35.2 nm. The synthesized nanocatalyst exhibited a very good catalytic ability in the synthesis reaction of pyran derivatives and 2-benzylidenemalononitrile derivatives. Product 2-amino-7,7-dimethyl-4-(4-nitrophenyl)-5-oxo-5,6,7,8-tetrahydrobenzo[*b*]pyran **4e** was achieved in 97% yield with a TON of 129.3 and a TOF of 646.6 h^{-1} and product 2-(4-cyanobenzylidene)malononitrile **3j** was achieved in 96% yield with a TON of 128 and a TOF of 984.6 h^{-1}. In addition, the synthesized nanocatalyst was easily separated from the reaction mixture by a magnet and used 7 consecutive times without significant loss of catalytic activity. Also, leaching of copper metal from the synthesized nanocatalyst was very insignificant for this reaction.

Received 18th August 2023
Accepted 23rd September 2023

DOI: 10.1039/d3ra05649j

rsc.li/rsc-advances

Introduction

Green chemistry is now a widely discussed subject, attracting the attention of numerous companies and researchers alike. The goal of green chemistry is to discover eco-friendly reaction conditions as well as enhance reaction rates and the elimination of dangerous chemicals and solvents in the application of chemical products. Additionally, green chemistry decreases the harm caused by chemical substances and processes to human health and effectively eliminates environmental pollution by implementing sustainable prevention initiatives. The use of catalysts is one of the principles of green chemistry. The prevention of waste production in the synthetic process is made possible by the utilization of catalysts and non-toxic reagents. Heterogeneous catalysts have become increasingly appealing in the synthetic organic field due to their ability to simplify product isolation, facilitate simple preparation methods, provide economic advantages, allow for recycling, and contribute to green procedures. Recently, the catalytic activity of nanocatalysts in various reactions, including the formation of new carbon–heteroatom and carbon–carbon bonds, was investigated.[1–3]

Fe_3O_4 nanoparticles have been extensively employed in the fields of catalysis.[4,5] Recently, there has been a surge in interest in utilizing magnetically responsive materials, specifically Fe_3O_4 MNPs, which are combined with nano-structured transition metal heterogeneous catalysts.[6] This approach has gained attention due to its environmental friendliness and the convenience it offers in terms of catalyst recyclability.[7] These systems offer enhanced flexibility, allowing for improved contact between the catalyst and reactants. Consequently, the catalyst's activity is greatly increased. Fe_3O_4 magnetic nanoparticles (MNPs) possess a cubic inverse spinel configuration, wherein the Fe element exists in both the Fe^{2+} and Fe^{3+} cationic.

[a]*Department of Chemistry, Faculty of Science, University of Zanjan, Zanjan 45371-38791, Iran. E-mail: aliramazani@znu.ac.ir; aliramazani@gmail.com; sobhan.rezayati@yahoo.com; sobhan.rezayati@znu.ac.ir; masoudkarimi67@gmail.com*

[b]*Department of Biotechnology, Research Institute of Modern Biological Techniques (RIMBT), University of Zanjan, Zanjan 45371-38791, Iran*

[c]*Department of Chemistry, Payame Noor University, PO BOX 19395-4697, Tehran, Iran. E-mail: ss.sajjadifar@gmail.com*

† Electronic supplementary information (ESI) available: Copies of FT-IR, ^{1}H NMR (250 MHz, $CDCl_3$ or DMSO-d_6) and ^{13}C NMR (62.5 MHz, $CDCl_3$ or DMSO-d_6) spectra of synthesized compounds. See DOI: https://doi.org/10.1039/d3ra05649j

Nonetheless, Fe_3O_4 MNPs, when synthesized, exhibit instability owing to their elevated surface energy, which tends to promote oxidation, decomposition and aggregation. To prevent these issues, a potential solution is to encase Fe_3O_4 NPs within a shell made of a different material. Silica functionalized magnetic nanoparticles have gained significant attention due to their numerous advantageous features, including ease of functionalization, lack of toxicity, straightforward synthesis, convenient separation from the reaction medium facilitated by an external magnet, and straightforward synthesis. Silica has become increasingly popular due to its attractive potential, making it one of the most durable and versatile surfaces. It offers numerous advantages including chemical inertness and biocompatibility, improved mechanical stability, thermal stability, optical transparency, and the ability to control chemical reactions spectroscopically.[8] We were motivated to develop green and sustainable Fe_3O_4-based heterogeneous catalysts due to the intriguing characteristics of these special. Scientists can design highly active, selective and flexible nanocatalysts. All these benefits make industrial chemical reactions more resource efficient, enabling energy use and waste reduction, helping to offset the environmental impact of reliance on chemical processes.[9,10]

From the point of view of green chemistry, it is very important to design and economic chemical processes using heterogeneous catalysts for the preparation of chemical and pharmaceutical products through multicomponent reactions (MCRs).[11–13] Multi-component reactions have significant advantages, such as high atom economy and bond formation efficiency, avoiding by-products, fast and simple execution, saving time and energy, and avoiding complex purification methods.[14]

Knoevenagel condensation is a nucleophilic addition reaction, in which a compound containing active hydrogen, such as malonates, which attacks a carbonyl group (aldehyde or ketone) and loses a water molecule to form the final product.

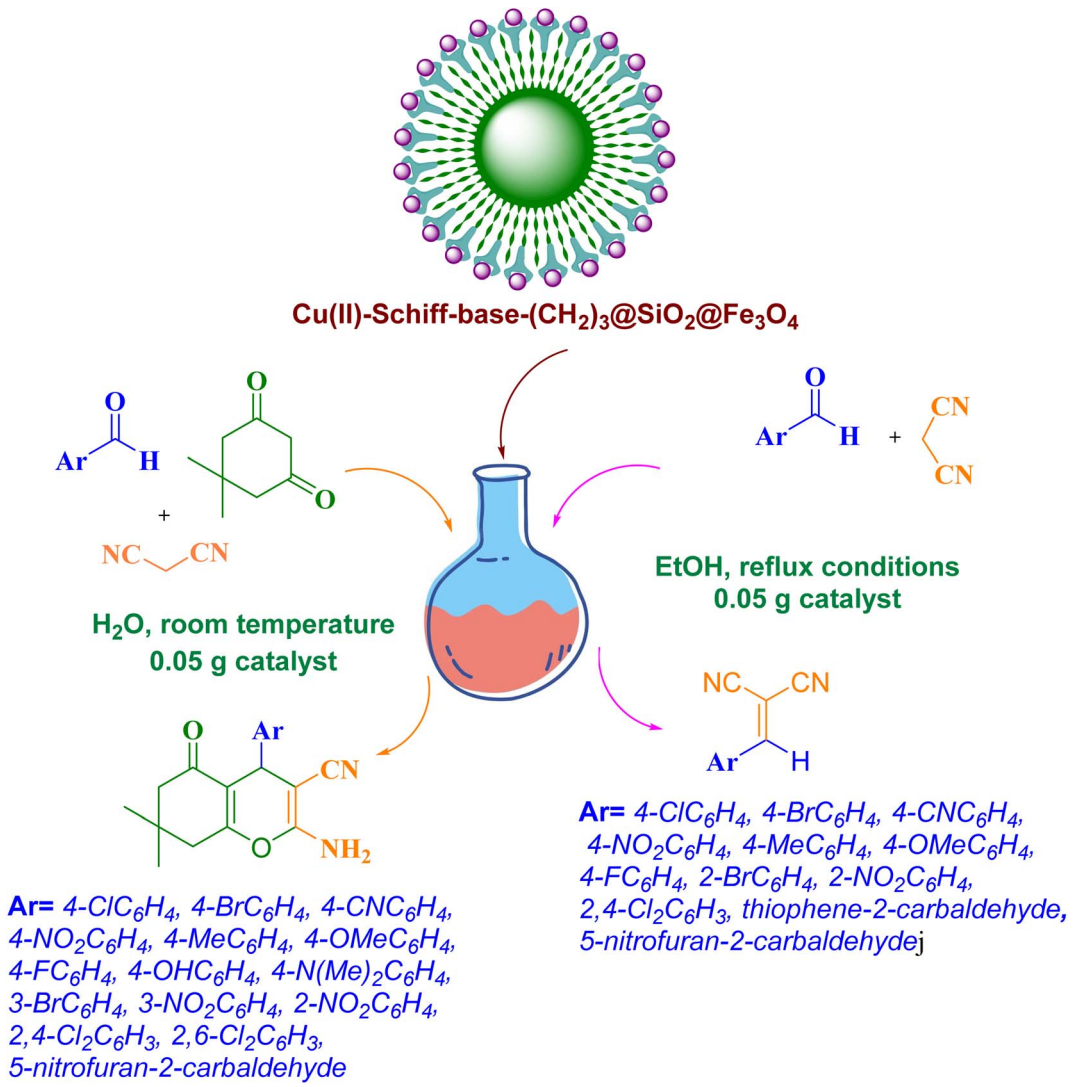

Scheme 1 Schematic representation of the 2-amino-4*H*-pyrans and 2-benzylidenemalononitrile derivatives catalyzed by Cu(II)-Schiff-base-$(CH_2)_3$@SiO_2@Fe_3O_4

Knoevenagel condensation is one of the most common methods used in organic chemistry for electron-less synthetic olefins, which occurs as a result of the reaction between active methylenes and carbonyl compounds.[15] The α,β-unsaturated compounds which formed by Knoevenagel condensation, are one of the essential intermediates in producing chemicals, herbicides, carbohydrates, pharmaceuticals, and pesticides, dyes.[16–19] Benzylidene malononitriles are regularly utilized as an intermediate molecule and a target molecule in organic synthesis. They have fascinated consideration due to special properties such as anti-fungal, anti-cancer, anti-bacterial, and anti-corrosive[20–23] and used to probes of solvent friction.[24]

Substituted 2-amino-4*H*-pyran derivatives in which the Knoevenagel condensation are prepared through a three-component one-pot reaction including malononitrile, aldehyde and enolizable acids (such as dimedone, barbituric acid, α,β-naphthols, 2-hydroxy-1,4-naphthoquinone-4-hydroxycoumarin).[25–27] Recently, the synthesis of this group of compounds has been revised due to the increase in their use in the field of medicinal chemistry and materials science.[28] In the past, various synthetic methods for making this class of compounds, including conventional thermal reactions,[29] microwave-radiation reactions[30] in the presence of organic solvents and various catalysts and such reactions have been widely expanded. Substituted 2-amino-4*H*-pyran derivatives are synthesized in the presence of various catalysts including theophylline,[31] uric acid,[32] $TiCl_4$,[33] Fe_3O_4@SiO_2@NH_2,[34] Fe_3O_4/HNTs,[35] Fe_3O_4@SiO_2-imine/phenoxy-Cu(II) core–shell MNPs,[36] lipase,[37] $CuFe_2O_4$@starch,[38] ZnO,[39] nano CeO_2,[40] Fe_3O_4@SiO_2@$(CH_2)_3$-Urea,[41] Fe_3O_4@SiO_2@GPTMS@guanidine,[42] Fe_3O_4@SiO_2@$(CH_2)_3$/EDA,[43] NH_2@SiO_2@Fe_3O_4,[44] Au/NiAlTi LDH,[45] core/shell Fe_3O_4@GA@isinglass.[46] However, the many disadvantages of using these catalysts, such as low efficiency, long reaction time, corrosiveness, environmental pollution, *etc.*, made chemists think of using novel catalysts to perform this reaction.

Considering the importance and benefits of MCRs with catalysts for the synthesis of heterocyclic compounds,[47] in this study, we synthesized for the first time the copper(II) complex containing pyridine-2-carbaldehyde ligand and its direct binding onto ethylenediamine functionalized with Fe_3O_4@SiO_2 nanoparticles [Cu(II)-Schiff base-$(CH_2)_3$-SiO_2@Fe_3O_4] as a recyclable catalysts by a facile and multi-step method. Then, the catalytic activity of this nanocatalyst has been investigated for the synthesis of 2-amino-4*H*-pyrans and 2-benzylidenemalononitriles (Scheme 1).

Experimental

Tools and chemicals

All reagents and solvents such as ethanol (C_2H_5OH), dry methanol (CH_3OH), acetone [$(CH_3)_2CO$], toluene ($C_6H_6CH_3$), aqueous ammonia 25% (NH_4OH), iron(II) sulfate ($FeSO_4 \cdot 7H_2O$), copper(II) nitrate trihydrate [$Cu(NO_3)_2 \cdot 3H_2O$], iron(III) chloride ($FeCl_3$), tetraethyl orthosilicate (TEOS, $SiC_8H_{20}O_4$), (3-chloropropyl)silanetriol ($C_3H_9ClO_3Si$), 2-picolylaldehyde (NC_5H_4-CHO), ethylenediamine [$C_2H_4(NH_2)_2$], various aromatic aldehydes, malononitrile ($C_3H_2N_2$), and dimedone ($C_8H_{12}O_2$) were purchased from the Fluka (Switzerland) or Merck Company. Infrared spectra were taken with a PerkinElmer 597 devices. ^{1}H-NMR and ^{13}C-NMR spectra were taken with Bruker 250 MHz and FT NMR-62.5 MHz devices in pure solvents ($CDCl_3$ and DMSO-d_6). Chemical shifts with scale δ are expressed in parts per million (ppm) and coupling constant with J in Hz. The splittings of ^{1}H-NMR peaks are characterized by singlet (s), doublet (d), triplet (t), quartet (q), multiplet (m), broad (br). Also, Electrothermal 9100 device was used to determine the melting point of the synthesized products. VSM analysis (Taban, Tehran, Iran) was used to determine the magnetic properties of the synthesized catalysts. In order to investigate the crystal structure of the prepared samples, an XRD machine (advanced diffractometer X'Pert-PRO works with 40 kV and 40 mA at room temperature) was used. In order to investigate the structure and determine the dimensions of nanoparticles prepared in this method, transmission electron microscope (TEM) model (Zeiss EM10C-80 KV) and scanning electron microscope (SEM) model (VEGA, TESCAN Czech Republic) were used. EDAX detector and X-ray map were used to determine the elemental analysis of the synthesized catalysts. Thermal gravimetric analysis (TGA) was performed by Setaram SETSYS 16/18 device from 25 to 800 °C with an increase of 10 °C per min.

The preparation of Cu(II)-Schiff base-$(CH_2)_3$-SiO_2@Fe_3O_4

Cu(II)-Schiff base-$(CH_2)_3$-SiO_2@Fe_3O_4 was effectively synthesized to the following steps (Scheme 2).

Preparation of Fe_3O_4 NPs

In this work for synthesis of Fe_3O_4, co-precipitation method was investigated. In summary, in 120 mL of de-ionized water, mixture of $FeSO_4 \cdot 7H_2O$ (0.9 g)/$FeCl_3$ (0.97 g) at 80 °C was prepared. Following this, a solution comprising NH_4OH 1.5 M (120 mL) was gradually added to the mixture under N_2 gas. Consequently, the mixture rapidly transitioned from a yellowish hue to a black color. The synthesized Fe_3O_4 was detached with an external magnet. Black Fe_3O_4 NPs were washed with deionized water (4 × 30 mL) to pH 7.5 and once with acetone (1 × 30 mL) for 5 times. Finally, the obtained black particles were placed in an oven at 40 °C for 24 h.[48]

Preparation of SiO_2@Fe_3O_4

In a 250 mL round-bottom flask, one gram of magnetite nanoparticles (Fe_3O_4) was added in 100 mL of a mixture of ethanol and deionized water (20 : 80) for 30 min in an ultrasonic to complete its dispersion. Then, TEOS (2 mL) and 25% ammonia (2 mL) were added to the mixture. Then it was stirred with a mechanical stirrer under nitrogen gas at room temperature for 12 h. The obtained SiO_2@Fe_3O_4 nanoparticles were washed five times with deionized water (4 × 30 mL) and finally once with ethanol (1 × 30 mL), and in each washing time, the nanoparticles were deposited using a magnet. The obtained nanoparticle was placed in an oven at a temperature of 40 °C for 24 h.[48]

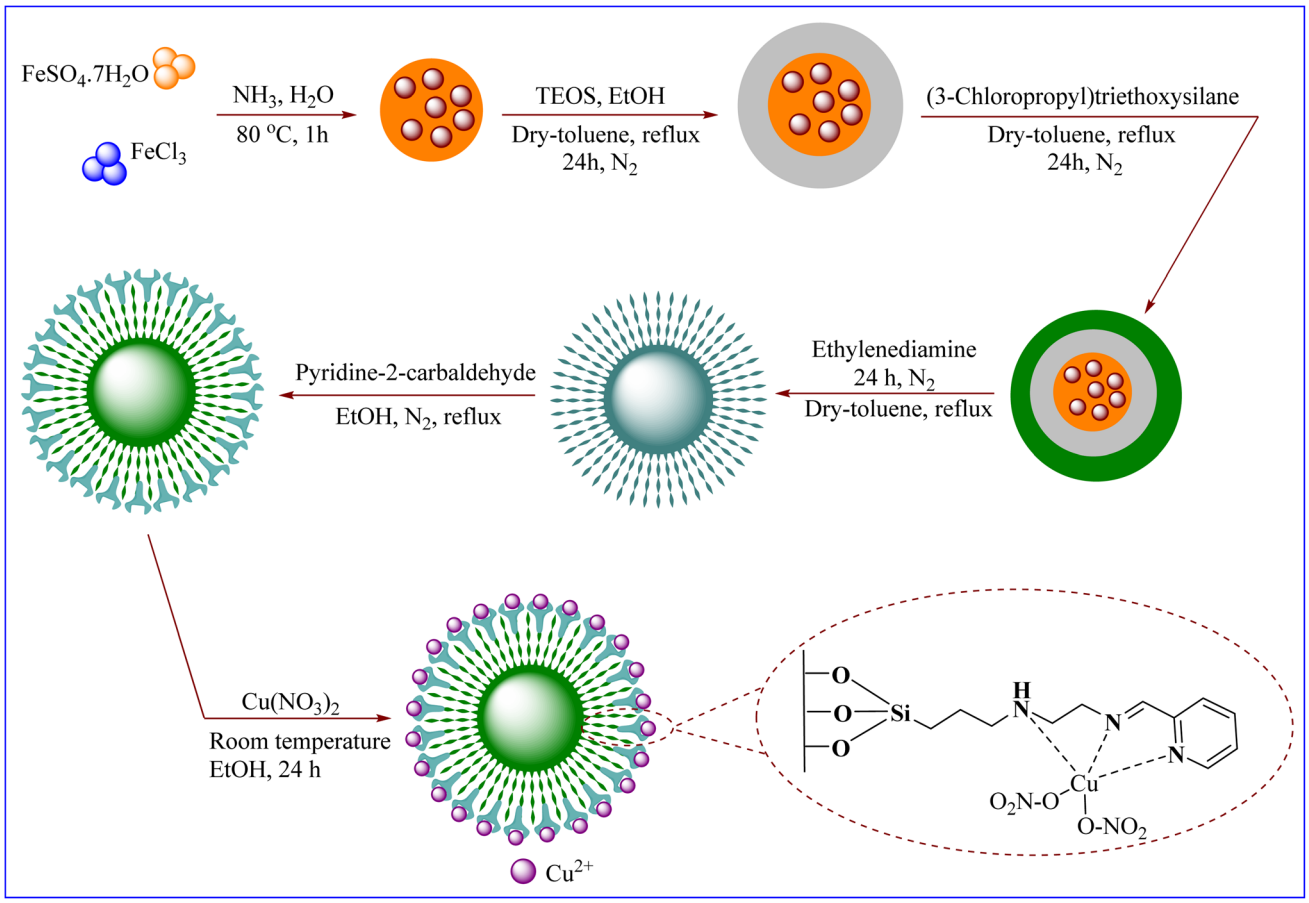

Scheme 2 Synthetic route of magnetic Cu(II)-Schiff-base-$(CH_2)_3$@SiO_2@Fe_3O_4

Preparation of $Cl(CH_2)_3$@SiO_2@Fe_3O_4

After dispersed of SiO_2@Fe_3O_4 NPs (1 g) in 100 mL of dry toluene, 10 mmol (3-chloropropyl)triethoxysilane was added it, and refluxed under N_2 for 24 h. The $Cl(CH_2)_3$@SiO_2@Fe_3O_4 was separated by an external magnetic field and washed with dry toluene and diethyl ether each twice times (2 × 30 mL). $Cl(CH_2)_3$@SiO_2@Fe_3O_4 dried overnight at room temperature.[48]

Preparation of $NH_2(CH_2)_2NH$-$(CH_2)_3$@SiO_2@Fe_3O_4

After dispersed of 1 g of $Cl(CH_2)_3$@SiO_2@Fe_3O_4 NPs in 100 mL of EtOH, the 0.72 g ethylenediamine slowly was added to it under N_2 atmosphere under reflux conditions for 24 h. The NPs was separated by an external magnetic field and washed with dry toluene (2 × 30 mL) and dried overnight at room temperature.

Preparation of Schiff-base-$(CH_2)_3$@SiO_2@Fe_3O_4

After dispersed of 1 g of $NH_2(CH_2)_2NH(CH_2)_3$@SiO_2@Fe_3O_4 NPs in 100 mL of dry ethanol, the 10 mmol pyridine-2-carbaldehyde was added to it under N_2 atmosphere under reflux conditions for 24 h. The Schiff-base-$(CH_2)_3$@SiO_2@Fe_3O_4 was separated by an external magnetic field and washed with dry toluene (2 × 30 mL) and dried overnight at room temperature.

Preparation of Cu(II)-Schiff-base-$(CH_2)_3$@SiO_2@Fe_3O_4

To prepare Cu(II)-Schiff-base-$(CH_2)_3$@SiO_2@Fe_3O_4, in a 250 mL round-bottomed flask 1 g of Schiff-base-$(CH_2)_3$@SiO_2@Fe_3O_4 was placed in an ultrasonic bath in 30 mL of ethanol for 30 min. Then, 2.5 mmol of copper nitrate solution in 10 mL of ethanol solvent was added to the reaction mixture and stirred for 48 h by a magnetic stirrer under reflux conditions. After finishing the reaction mixture was cooling in room temperature. The next steps, the contents were transferred to a beaker. The obtained Cu(II)-Schiff-base-$(CH_2)_3$@SiO_2@Fe_3O_4 were washed three times (20 × 3 mL) with ethanol, and in each washing, the nanoparticles were deposited using a magnet and the supernatant solution was overflowed. In order to dry the obtained nanoparticles, it was set at room temperature for 24 h.

General procedure for the synthesis of 2-amino-4*H*-pyran derivatives

For this reaction, a mixture of dimedone, aromatic aldehyde, malononitrile (1 : 1 : 1 mmol ratio), 0.05 g nanocatalyst, and 3 mL ethanol was added in a round bottom flask under reflux conditions. The progress of the reaction was evaluated by thin layer chromatography (TLC). After completing the reaction, the mixture was cooled, then nanocatalyst filtered separated by external magnetic field. The 2-amino-4*H*-pyran derivatives can

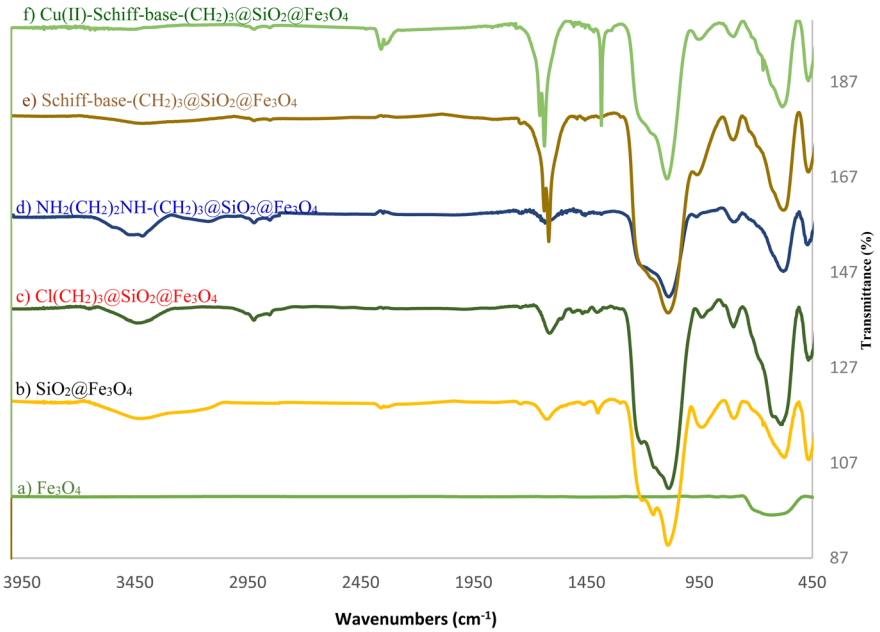

Fig. 1 FT-IR spectra of (a) Fe_3O_4, (b) $SiO_2@Fe_3O_4$, (c) $Cl(CH_2)_3@SiO_2@Fe_3O_4$, (d) $NH_2(CH_2)_2NH\text{-}(CH_2)_3@SiO_2@Fe_3O_4$, (e) Schiff-base-$(CH_2)_3@SiO_2@Fe_3O_4$, and (f) Cu(II)-Schiff-base-$(CH_2)_3@SiO_2@Fe_3O_4$

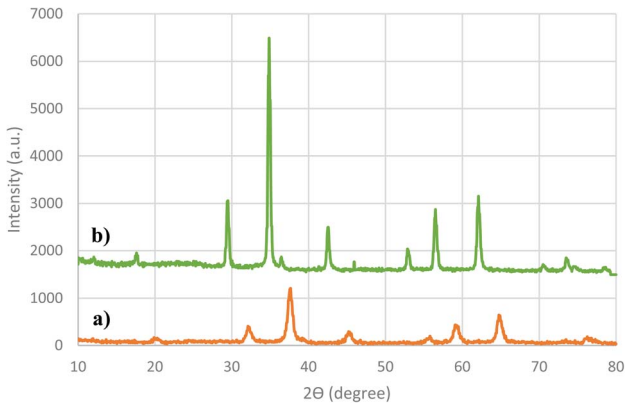

Fig. 2 PXRD patterns of (a) Fe_3O_4 and (b) Cu(II)-Schiff-base-$(CH_2)_3@SiO_2@Fe_3O_4$

be recrystallized by hot ethanol. The structures of compounds **4a–p** were apparent from the FT-IR, ^{1}H NMR and ^{13}C NMR spectra.

General procedure for the synthesis of 2-benzylidene malononitriles

For this reaction, a mixture of 1 mmol of various aromatic aldehyde, 1 mmol of malononitrile, 3 mL distilled water, and 0.05 g of nanocatalyst was added to a round-bottomed balloon and was stirred at room temperature for suitable times. The progress of the reaction was evaluated by thin layer chromatography (TLC). After completing the reaction, the mixture was cooled, then nanocatalyst filtered separated by external magnetic field. The 2-benzylidene malononitrile derivatives can be recrystallized by hot ethanol. The structures of compounds **3a–m** were apparent from the FT-IR, ^{1}H NMR and ^{13}C NMR spectra.

Table 1 The PXRD data for the Cu(II)-Schiff-base-$(CH_2)_3@SiO_2@Fe_3O_4$

Entry	2θ	Peak width (FWHM)	Miller indices			Particle size (nm)	Inter-planer distance (nm)
			h	*k*	*l*		
1	18.42	0.3444	0	1	2	23.4	0.3686
2	30.16	0.2952	1	0	4	27.9	0.2703
3	35.51	0.3444	1	1	0	24.2	0.2519
4	43.25	0.2952	2	0	2	29.0	0.2080
5	46.65	0.1476	0	2	4	58.5	0.1842
6	53.59	0.1968	1	1	6	45.2	0.1696
7	57.17	0.3444	1	2	2	26.3	0.1601
8	62.75	0.2400	2	1	4	38.8	0.1487
9	74.23	0.2460	2	2	0	40.5	0.1259

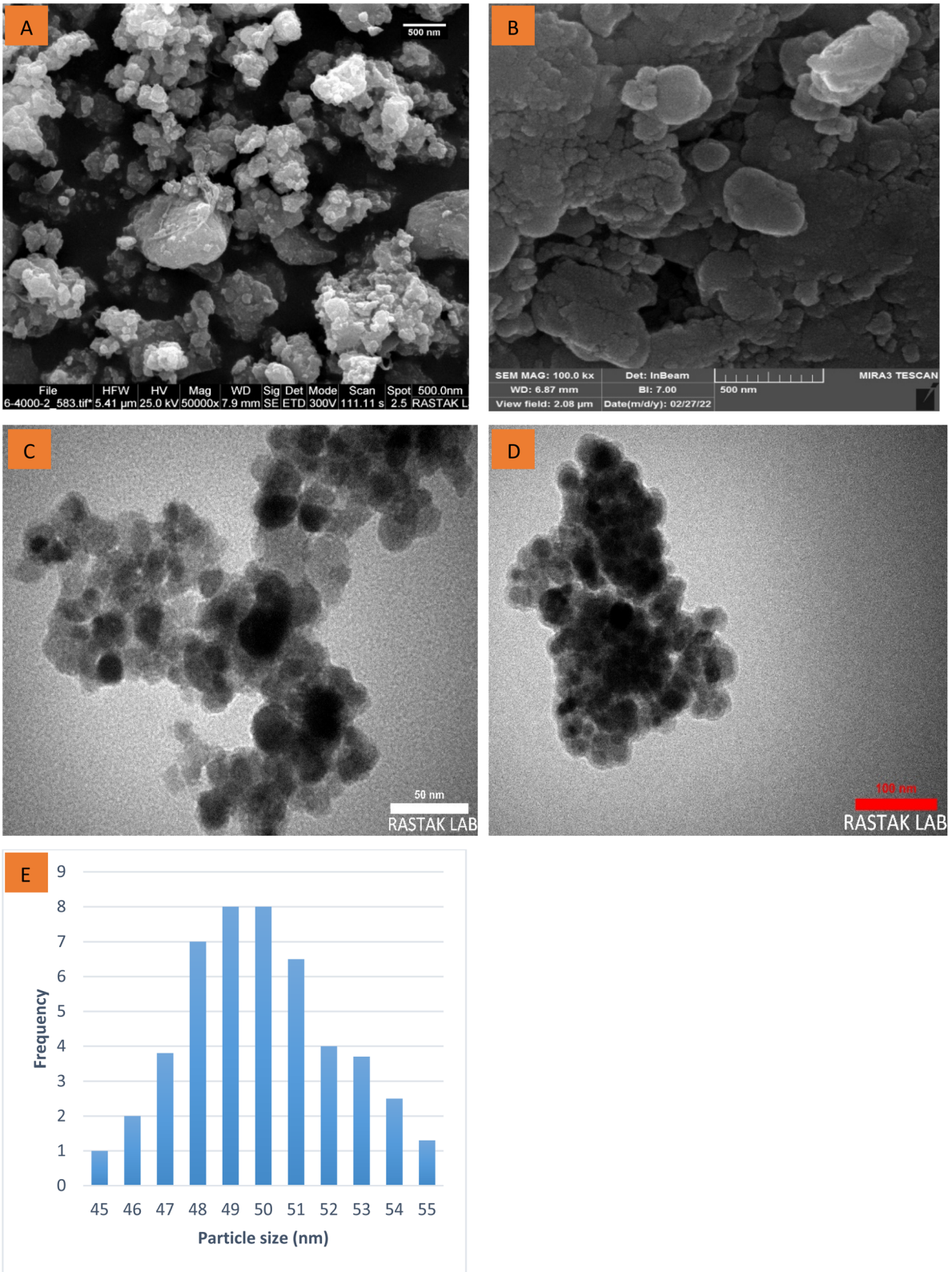

Fig. 3 FE-SEM images of the (A) Fe_3O_4 and (B) as-prepared nanocatalyst, TEM images of the (C) Fe_3O_4 and (D) as-prepared nanocatalyst, (E) particle size distribution diagram of as-prepared nanocatalyst.

Results and discussions

In this study, we have synthesized the Cu(II)-Schiff-base-$(CH_2)_3$@SiO_2@Fe_3O_4 with a facile and multi-step method (Scheme 2). In this regard, silica-coated iron oxide was prepared *via* TEOS in the presence of iron oxide. Then, the surfaces of the synthesized magnetic nanocatalyst in the pervious step are immobilized with (3-chloropropyl)triethoxysilane and ethylenediamine, respectively to afford the $NH_2(CH_2)_2NH$-$(CH_2)_3$@SiO_2@Fe_3O_4. In the following, the synthesized magnetic nanocatalyst in the pervious step reacted with pyridine-2-carbaldehyde and treatment with copper nitrate to synthesis of final catalyst.

The structure and the functional groups of (a) Fe_3O_4, (b) SiO_2@Fe_3O_4, (c) $Cl(CH_2)_3$@SiO_2@Fe_3O_4, (d) $NH_2(CH_2)_2NH$-$(CH_2)_3$@SiO_2@Fe_3O_4, (e) Schiff-base-$(CH_2)_3$@SiO_2@Fe_3O_4, and (f) Cu(II)-Schiff-base-$(CH_2)_3$@SiO_2@Fe_3O_4 were approved by the FT-IR spectrum (Fig. 1). By examining layer by layer and comparing with the new layer, we can prove the synthesis of the catalyst. Fe_3O_4 NPs is confirmed *via* Fe–O bond apparition around 615 cm^{-1} (Fig. 1a).[48] In the next step, by coating SiO_2 two broad bands related to the hydroxyl groups and Si–O–Si appeared (Fig. 1b). Symmetric and antisymmetric stretching vibrations of Si–O–Si appeared about 795 and 1084 cm^{-1}, respectively.[48] Absorptions peaks of C–H group of $Cl(CH_2)_3$@SiO_2@Fe_3O_4 appeared about 2913 cm^{-1} (Fig. 1c). The absorptions peaks about 1619 and 3406 cm^{-1} that are belong to the bending vibration of N–H and stretching frequency of N–H, respectively[1] (Fig. 1d).[48] After adding pyridine-2-carbaldehyde absorptions peaks C=C belong to aromatic ring appear about in 1617 cm^{-1} and 1623 cm^{-1} (Fig. 1e). In Cu(II)-Schiff-base-$(CH_2)_3$@SiO_2@Fe_3O_4, the carbonyl peak shifts from 1636 cm^{-1} which indicates the complexation of Cu has occurred (Fig. 1f). The absorption peaks at about 1384 cm^{-1} belong to the bending vibration of NO_2.

PXRD analysis was used to identify the crystallite size, inter-planer distance and Miller indices of the nanocatalyst. Fig. 2 indicated the PXRD pattern of the Fe_3O_4 and Cu(II)-Schiff-base-$(CH_2)_3$@SiO_2@Fe_3O_4 were demonstrated in the 2θ at room temperature (range of 10–80°). Examining the X-ray diffraction pattern in the Fe_3O_4 shows seven index peaks at $2\theta = 19.9$, 32.4, 37.7, 44.9, 55.7, 59.7 and 65.1, which are respectively related to pages (1 1 1), (2 2 0), (3 1 1), (4 0 0), (4 2 2), (5 1 1) and (4 4 0), which agrees with the spectrum of Fe_3O_4 (JCPDS 88-0866) and confirms its cubic structure.[49] Moreover, examining the X-ray diffraction pattern in the Cu(II)-Schiff-base-$(CH_2)_3$@SiO_2@Fe_3O_4 shows new two peaks at $2\theta = 43.2$ (2 0 0) and 74.2 (2 2 0) that agrees with the spectrum of copper (JCPDS, copper file no. 04-0836). Two new peaks confirmed that the nanoparticles successful synthesized. Additionally, we evaluated the crystallite size and inter-planer distance of the catalyst for per peak of intensity by applying the Scherrer equation [$D = K\lambda/(\beta \cos \theta)$]

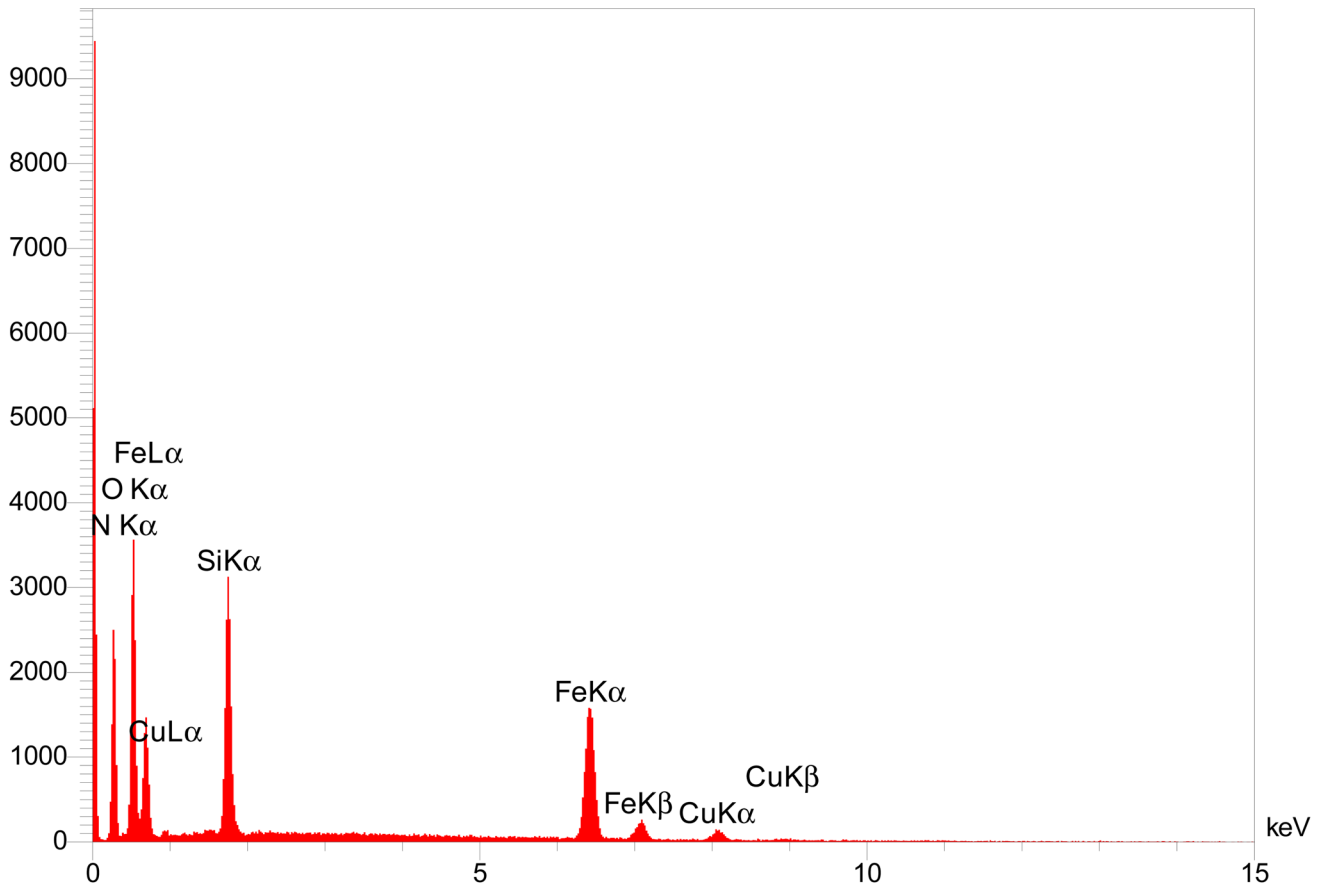

Fig. 4 The EDX spectrum of the Cu(II)-Schiff-base-$(CH_2)_3$@SiO_2@Fe_3O_4.

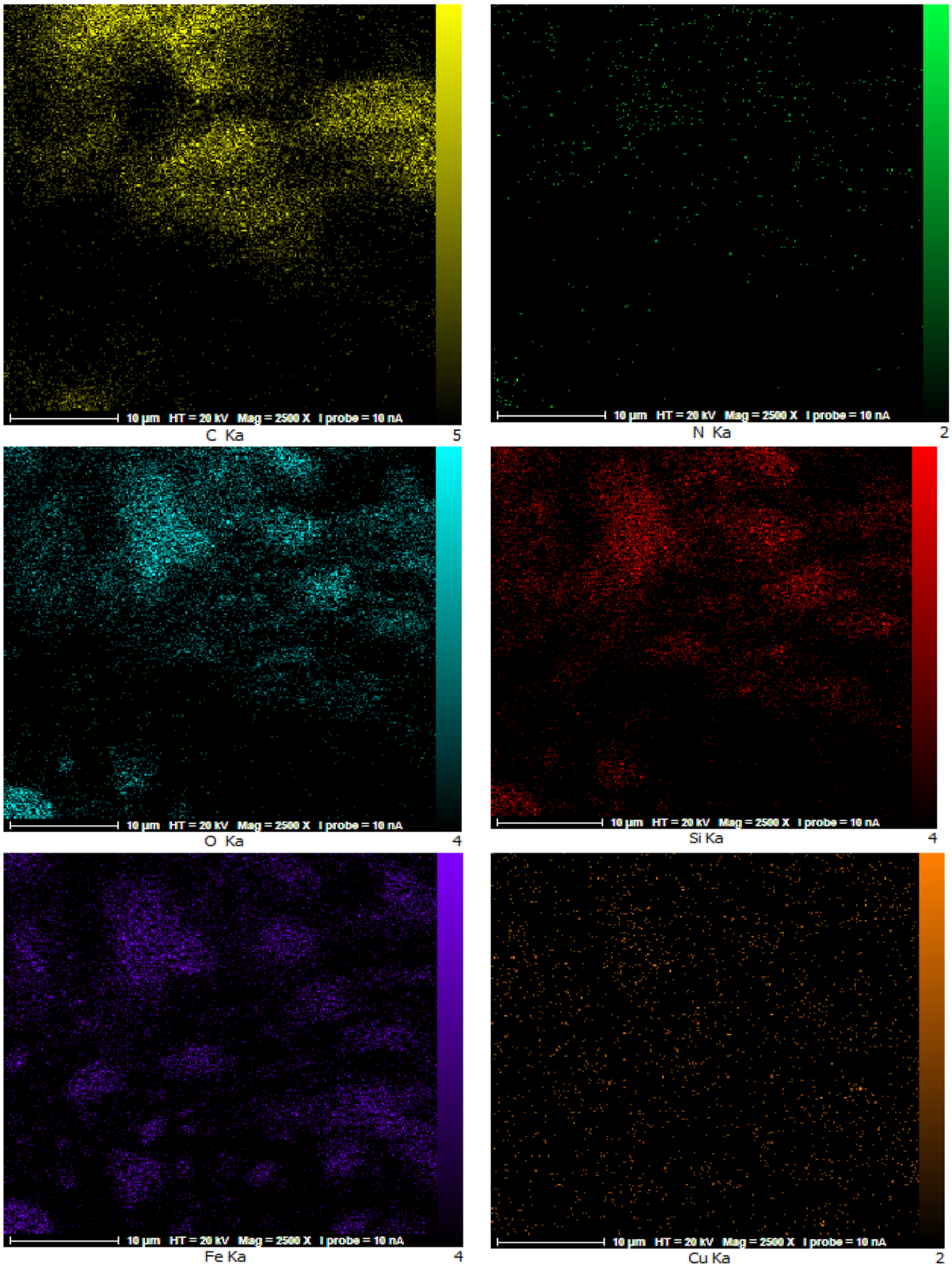

Fig. 5 Corresponding elemental mapping of as-prepared nanocatalyst.

and Bragg formula [$d_{hkl} = k/(2 \sin \theta)$], respectively (Table 1). The Table 1 shows that the average crystallite size was 35.2 nm and average inter-planer distance was 0.2097 nm.

The major physical features and surface morphology of the Fe_3O_4 and as-prepared nanocatalyst were considered by FE-SEM images in various magnifications (Fig. 3A and B). The SEM

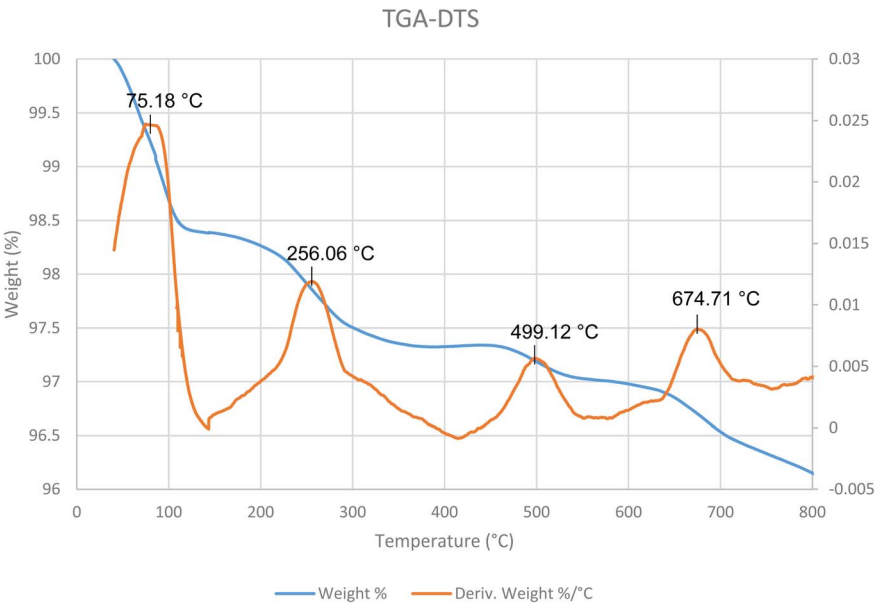

Fig. 6 The TGA-DTS analysis of the as-prepared nanocatalyst.

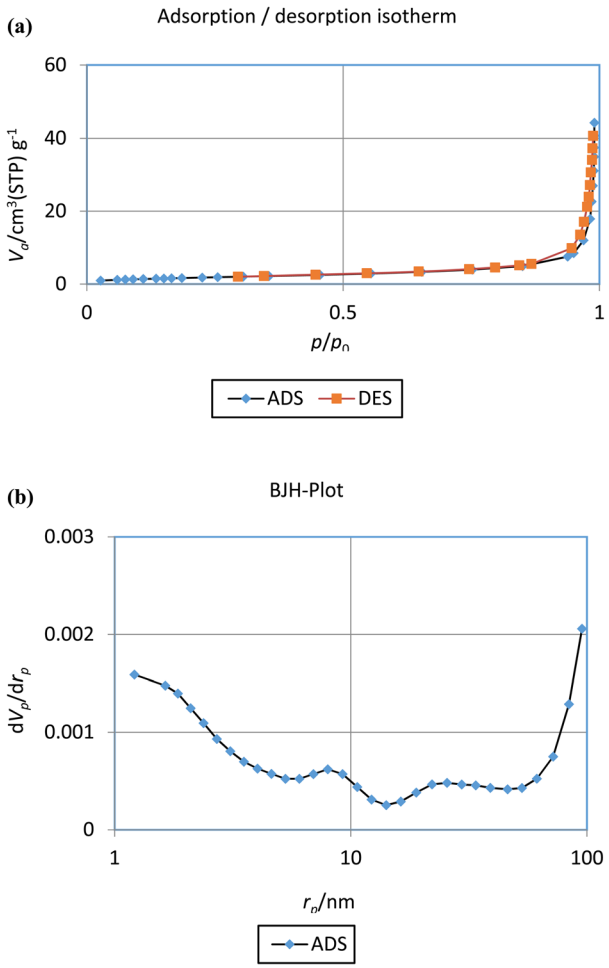

Fig. 7 The (a) BET plot of the nitrogen adsorption–desorption and (b) pore size distribution curve of the as-prepared nanocatalyst.

Table 2 BET results of Cu(II)-Schiff-base-$(CH_2)_3$@SiO_2@Fe_3O_4

Entry	Parameter	Amount
1	Pore volume	1.4717 [cm^3(STP) g^{-1}]
2	BET surface area ($a_{s,BET}$)	41.4054 [m^2 g^{-1}]
3	Total pore volume($p/p_0 = 0.990$)	0.066146 [cm^3 g^{-1}]
4	Mean pore diameter	41.306 [nm]

images display that the Fe_3O_4 and as-prepared nanocatalyst have a spherical shape with nanoscale dimensions. After coating Fe_3O_4 with silica and various organic compounds, the spherical morphology of as-prepared nanocatalyst was intact. In another study, TEM images for Fe_3O_4 and as-prepared nanocatalyst were studied (Fig. 3C and D). The TEM analysis images confirm well and show the core–shell structure. TEM enlarged

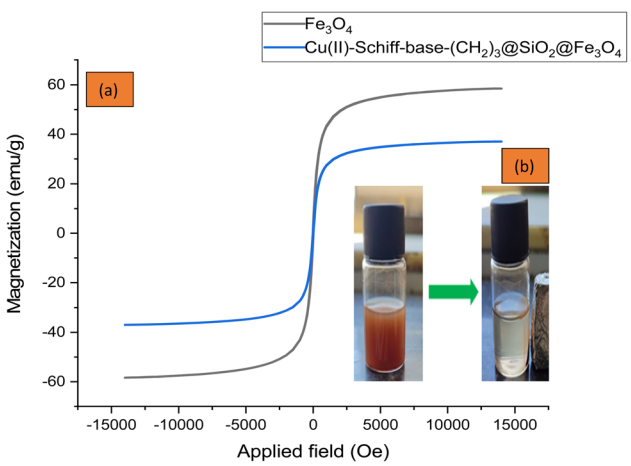

Fig. 8 The VSM analysis of the (a) Fe_3O_4 and (b) Cu(II)-Schiff-base-$(CH_2)_3$@SiO_2@Fe_3O_4 nanocatalyst.

Table 3 Investigation of optimal conditions in the presence of Cu(II)-Schiff-base-$(CH_2)_3$@SiO_2@Fe_3O_4 for pyran synthesis[a]

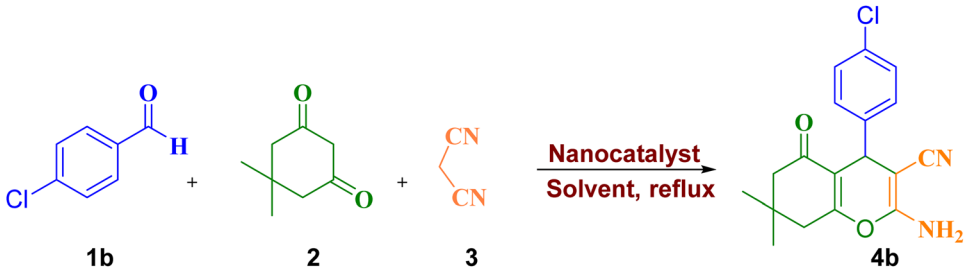

1b 2 3 4b

Entry	Amount of catalyst (g)	Solvent (2 mL)	Time (min)	Yield[b] (%)
1	—	Ethanol	5 h	Nil
2	0.005	Ethanol	60	55
3	0.01	Ethanol	60	71
4	0.03	Ethanol	45	82
5	0.05	Ethanol	40	94
6	0.07	Ethanol	40	91
7	0.09	Ethanol	40	90
8	0.1	Ethanol	45	88
9	0.05	CH_3CN	100	66
10	0.05	$CHCl_3$	90	75
11	0.05	CH_2Cl_2	90	76
12	0.05	CH_3OH	120	70
13	0.05	Toluene	180	65

[a] Reaction conditions: 4-chlorobenzaldehyde (1 mmol), dimedone (1 mmol), malononitrile (1 mmol), reflux conditions. [b] Isolated pure yield.

form clearly shows that silica has been successfully fixed (bright layer) on Fe_3O_4 magnetic nanoparticles (dark area). Moreover, the particle size distribution diagram for as-prepared nanocatalyst are almost 45–55 nm (Fig. 3E).

The elemental composition related to as-prepared nanocatalyst was examined by EDX analysis (Fig. 4). Hence, the presence of nanocatalyst components elements, including Fe, Cu, Si, O, C, and N and the mass percentages 14.04, 1.62, 15.40, 37.46, 29.40, and 2.08, respectively was proved as expected. This analysis show that the copper metal coated well on the surface. The results obtained from the ICP analysis show that the exact amount of copper in the structure is 1.92 w%.

Table 4 Comparison of catalytic activity of a variety of catalysts for the Knoevenagel–Michael cyclocondensation for the synthesis of **4b**

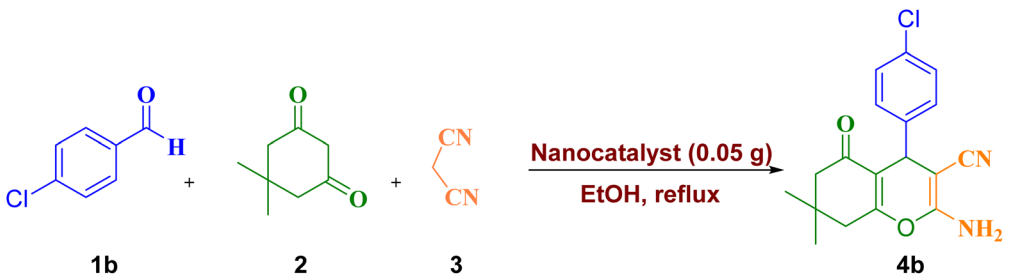

1b 2 3 4b

Entry	Catalyst	Conditions	Yield[a] (%)
1	Fe_3O_4	Ethanol/reflux	50
2	SiO_2@Fe_3O_4	Ethanol/reflux	40
3	Cl-$(CH_2)_3$@SiO_2@Fe_3O_4	Ethanol/reflux	Trace
4	$NH_2(CH_2)_2NH$-$(CH_2)_3$@SiO_2@Fe_3O_4	Ethanol/reflux	95
5	Schiff-base-$(CH_2)_3$@SiO_2@Fe_3O_4	Ethanol/reflux	22
6	Cu(II)-Schiff-base-$(CH_2)_3$@SiO_2@Fe_3O_4	Ethanol/reflux	94

[a] Isolated pure yield.

Table 5 Reaction scope[a]

Entry	Product	Time (min)	Yield[b] (%)	TON	TOF (h^{-1})	M_p (reference)
1	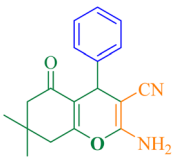 **4a**	40	94	125.3	189	229–231 (ref. 50)
2	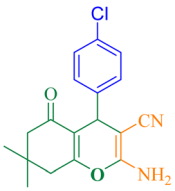 **4b**	20	95	126.6	383	212–214 (ref. 50)
3	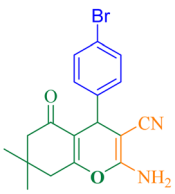 **4c**	20	94	125.3	379.6	215–217 (ref. 50)
4	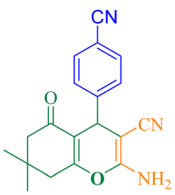 **4d**	12	96	128	640	222–224 (ref. 50)
5	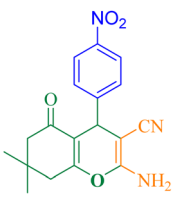 **4e**	12	97	129.3	646.6	178–180 (ref. 50)
6	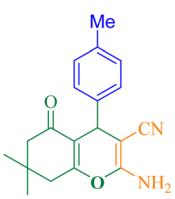 **4f**	40	94	125.3	189.8	215–217 (ref. 50)
7	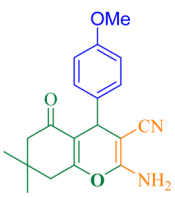 **4g**	40	92	122.6	185.6	196–198 (ref. 50)

Table 5 (*Contd.*)

Entry	Product	Time (min)	Yield[b] (%)	TON	TOF (h^{-1})	M_p (reference)
8	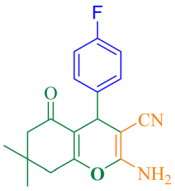 **4h**	20	90	120	363.6	188–190 (ref. 50)
9	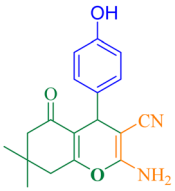 **4i**	45	89	118.6	158.1	220–222 (ref. 50)
10	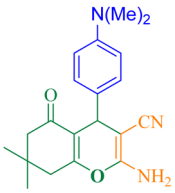 **4j**	35	94	125.3	216	185–187 (ref. 50)
11	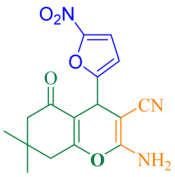 **4k**	10	95	126.6	791.2	153–155 (ref. 50)
12	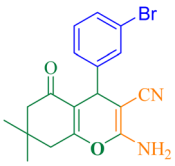 **4l**	25	93	124	302.4	212–214 (ref. 5)
13	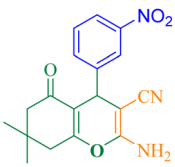 **4m**	15	92	122.6	490.4	211–213 (ref. 50)
14	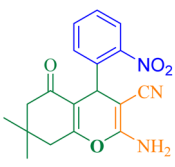 **4n**	12	96	128	640	222–224 (ref. 50)

Table 5 (*Contd.*)

Entry	Product	Time (min)	Yield[b] (%)	TON	TOF (h^{-1})	M_p (reference)
15	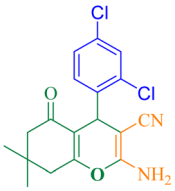 **4o**	30	91	121.3	242.6	180–182 (ref. 50)
16	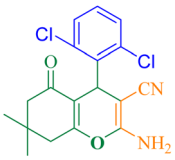 **4p**	30	92	122.6	245.3	248–250 (ref. 50)

[a] A mixture of various aldehyde (1 mmol), dimedone (1 mmol), malononitrile (1 mmol), catalyst (0.05 g, 0.75 mol%) in ethanol (2 mL) was refluxed. [b] Isolated pure yield.

In the following, elemental mapping analysis was used for determine the elemental content of the surface of catalyst. The distribution of atoms (Fe, Cu, Si, O, C, and N elements) indicates the position of the components associated with them and, distribution of components in catalyst (Fig. 5). The mapping images obtained demonstrate the presence of a significant concentration of C, O, and Fe elements originating from the catalyst support. According to this analysis, these elements make up over 80.9% of the sample. Furthermore, the mapping images clearly demonstrate a remarkable distribution of C, Si, N, and Cu moieties across the Fe_3O_4 support. These photograms clearly show that the distribution patterns of these elements agree well. This indicates that the imine groups of the as-prepared nanocatalyst serve as donor nitrogen atoms to coordinate with Cu(II) ions.

The thermal stability of as-prepared nanocatalyst was investigated by TGA-DTS curves by illustrate the nanocatalyst's weight loss and decomposition temperature (Fig. 6). As can be seen, three mass losses were confirmed for the nanocatalyst. The primary step is related to as mass-loss (1.8%) due to organic solvents or moisture at temperatures below 256 °C. The second mass-loss stage is occurred at temperatures below 500 °C due to the decomposition of organic compounds that coated on the surface. The third mass reduction occurred between 499–674 °C temperature. This decrease is because of the decomposition of silanol groups in as-prepared nanocatalyst. According to these results, the good thermal stability for the nanocatalyst was observed.

For appraise the textural properties and porosity of the Cu(II)-Schiff-base-$(CH_2)_3$@SiO_2@Fe_3O_4 the BET analysis was perform at 77 K by nitrogen adsorption–desorption (Fig. 7). The BET results from the adsorption–desorption isotherm and BJH curve are listed in Table 2. The mesoporous nanocatalyst display a type IV isotherm. The mean pore diameter of as-synthesized nanocatalyst was 41.31 nm. The surface area is 41.40 $m^2\ g^{-1}$, and the total pore volume is 0.066 $cm^3\ g^{-1}$.

The magnetic properties of Fe_3O_4 and Cu(II)-Schiff-base-$(CH_2)_3$@SiO_2@Fe_3O_4 nanoparticles were investigated by vibrating sample magnetometer (VSM) and are shown in Fig. 8. This analysis shows the magnetization curve of the samples at room temperature and in the fields of −10 000 to 10 000 Oe. The saturation magnetization (M_s) value of Fe_3O_4 and Cu(II)-Schiff-base-$(CH_2)_3$@SiO_2@Fe_3O_4 complex was 58.5 and 37 emu g^{-1}, respectively (Fig. 8a). This decrease in the saturation magnetization value is because of adding silica and other organic compounds on the surface of Fe_3O_4. The presence of a magnetic field shows that we have a clear decrease in the saturation magnetization of nanoparticles (Fig. 8b). This result is due to the effect of the magnetic field on the orientation of the magnetic dipoles. During the formation of magnetic nanoparticles, part of the nanoparticles aligns with the magnetic field.

Application of Cu(II)-Schiff-base-$(CH_2)_3$@SiO_2@Fe_3O_4

The use of Cu(II)-Schiff-base-$(CH_2)_3$@SiO_2@Fe_3O_4 catalyst due to its special properties can lead to a tremendous progress in the use of this material for various synthesis purposes. Moreover, the very low toxicity of this substance has made its use in chemistry as a green condition for us. We investigated the role and effect of this magnetically recoverable Cu(II)-Schiff-base-$(CH_2)_3$@SiO_2@Fe_3O_4 catalyst in the Knoevenagel–Michael cyclocondensation for the synthesis of 2-amino-4*H*-pyrans derivatives of various aromatic arylaldehyde, dimedone and malononitrile (Scheme 1). In order to optimize reaction conditions of **4b**, the effect of different parameters such as various amounts of nanocatalyst (0.05–0.1 g) and solvents (EtOH, CH_2Cl_2, CH_3CN, CH_3OH, Toluene, and $CHCl_3$) in the reaction of 4-chlorobenzaldehyde (1 mmol), malononitrile (1 mmol), and

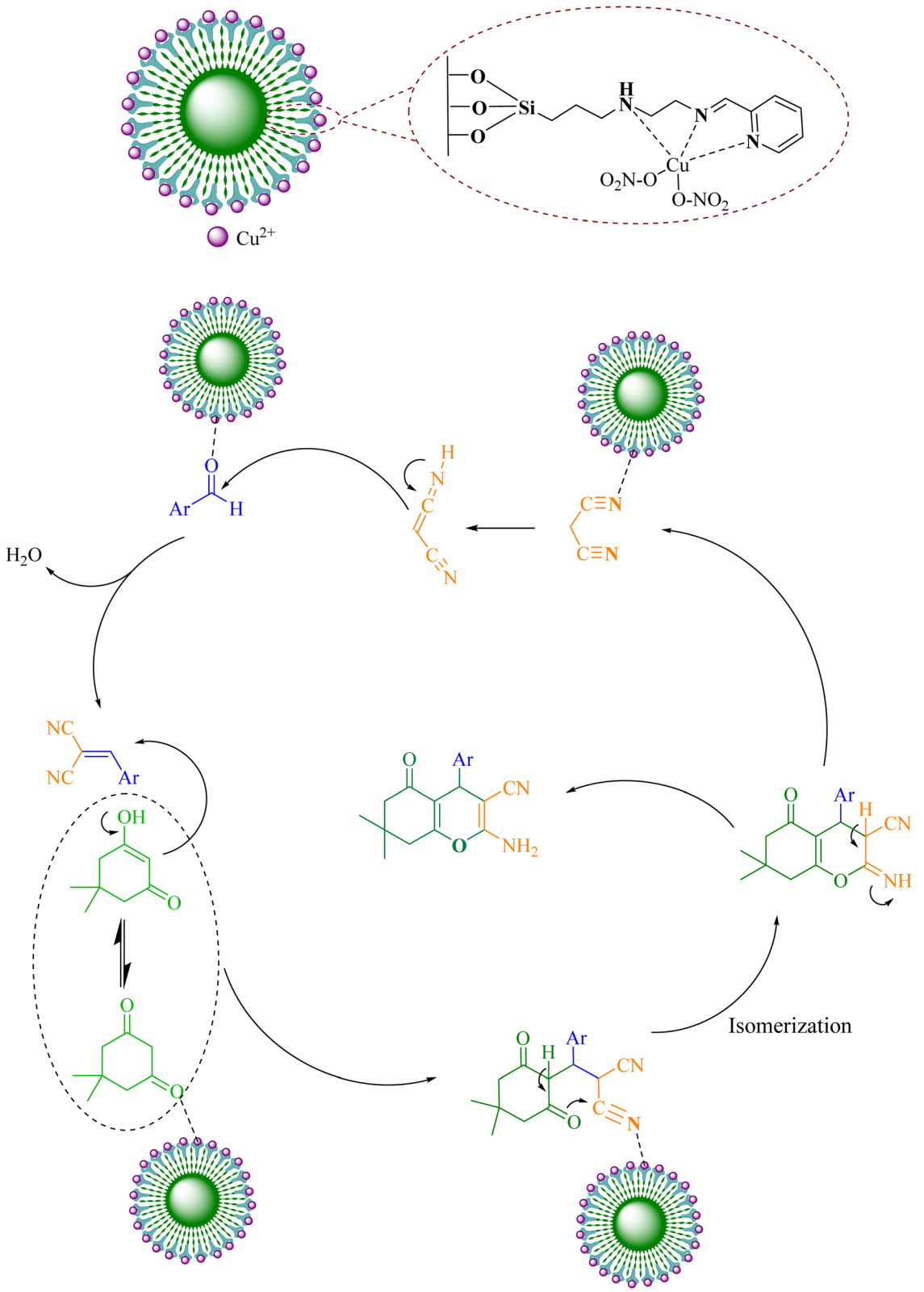

Scheme 3 A plausible mechanism for synthesis of 2-amino-4*H*-pyrans derivatives.

dimedone (1 mmol) was selected as model reaction. As the results of the optimization of the reaction conditions show, no product was obtained in the absence of the catalyst in ethanol after 5 h (Table 3, entry 1). The results in the presence of the catalyst were encouraging. In the presence of 0.005 g of catalyst, 55% of **4b** was obtained in ethanol under refluxing conditions

Table 6 Investigation of optimization of the reaction conditions for the Knoevenagel condensation[a]

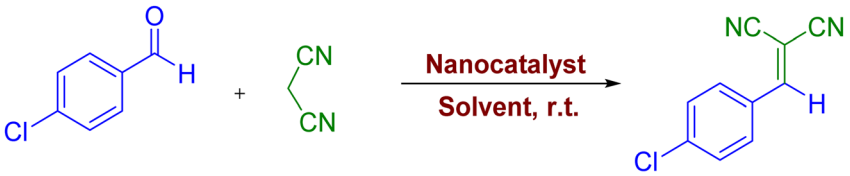

1b 2 3b

Entry	Catalyst (g)	Solvent	Temperature (°C)	Time (min)	Yield[b] (%)
1	—	—	25	180	Trace
2	0.005	Distilled water	25	60	55
3	0.01	Distilled water	25	30	78
4	0.03	Distilled water	25	30	85
5	0.05	Distilled water	25	20	95
6	0.07	Distilled water	25	25	90
7	0.09	Distilled water	25	25	89
8	0.1	Distilled water	25	40	84
9	0.05	CH_3CN	25	50	60
10	0.05	$CHCl_3$	25	50	65
11	0.05	CH_2Cl_2	25	50	74
12	0.05	CH_3OH	25	40	51
13	0.05	Toluene	25	100	38
14	0.05	EtOH	25	30	85
15	0.05	Distilled water	100 (reflux)	90	70

[a] Reaction conditions: malononitrile (1 mmol), 4-chlorobenzaldehyde (1 mmol), solvent (2 mL). [b] Isolated pure yield.

(Table 3, entry 2). 0.05 g of the nanocatalyst in ethanol under reflux conditions produces a higher yield of the product in a short time (Table 3, entry 5). It was observed that by increasing the amount of catalyst from 0.07 to 0.1 g, no improvement was observed (Table 3, entries 6–8). When the reaction was performed in other solvents, **4b** was obtained in lower yield (Table 3, entries 9–13).

Most importantly, the catalytic activity was investigated with other catalysts including Schiff-base-$(CH_2)_3$@SiO_2@Fe_3O_4, $NH_2(CH_2)_2NH$-$(CH_2)_3$@SiO_2@Fe_3O_4, Cl-$(CH_2)_3$@SiO_2@Fe_3O_4, SiO_2@Fe_3O_4, and Fe_3O_4. For this purpose, the reaction of 4-chlorobenzaldehyde (1 mmol), malonontrile (1 mmol) and dimedone (1 mmol) in the presence of 0.05 g of as-prepared nanocatalyst in ethanol under reflux conditions was investigated. The summary of the obtained results is presented in Table 4. As the table shows, Cu(II)-Schiff-base-$(CH_2)_3$@SiO_2@Fe_3O_4 shows better results than other catalysts and the corresponding product was obtained in 94% efficiency.

The reaction of various aromatic aldehydes with malononitrile and dimedone was investigated in the presence of nanocatalyst in ethanol and under reflux conditions (Table 5). As can be seen, from the reaction between different aldehydes containing electron-donating and electron-withdrawing groups, the desired products were obtained with an excellent yield of 89–97% after 10–40 min. The presence of electron-withdrawing groups (EWG) on the aromatic ring increased the rate of reaction, whereas the electron-donating groups (EDG) decreased the rate slightly.

Various mechanisms have been proposed for this reaction in recent years. Recently, due to the increase in the use of Lewis acids and positive halogen generating sources for this synthesis, more acceptable mechanisms have been proposed. Hence, a proposed and acceptable mechanism for the synthesis of pyran derivatives using a recyclable magnetic catalyst in the condition in EtOH at reflux condition is shown in Scheme 3. What is clear is that from the first stage of the reaction to the end of the reaction, the Lewis acid makes the nucleophilic groups more active and increases their electron deficiency (**I**), as a result, the nucleophile attacks faster and finally leads to ring closure. In the next step Michael addition of dimedone to arylidene malononitrile gives intermediate (**II**). Finally, isomerization gives the corresponding product (**III**).[51]

Using the good results obtained for the synthesis of 2-amino-4*H*-pyrans derivatives, we decided to investigate the activity of the synthesized catalyst for the synthesis of 2-benzylidenemalononitrile derivatives through the one-pot reaction of aromatic aldehydes and malonontrile. In order to optimize reaction conditions of **3b**, the effect of different parameters such as various amounts of nanocatalyst (0.05–0.1 g) and solvents (distilled water, CH_3CN, $CHCl_3$, CH_2Cl_2, and CH_3OH) in the reaction of 4-chlorobenzaldehyde (1 mmol) and malononitrile (1 mmol) was selected as model reaction. As the results of the optimization of the reaction conditions show, no product was obtained in the absence of the catalyst and solvent at room temperature after 180 min (Table 6, entry 1). The summary of the obtained results is presented in Table 6. As the table shows,

Table 7 Reaction scope[a]

Entry	Product	Time (min)	Yield[b] (%)	TON	TOF (h^{-1})	Reference
1	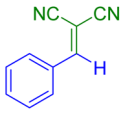 **3a**	20	95	126.6	383.8	80–82 (ref. 52)
2	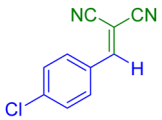 **3b**	15	94	125.3	501.3	163–165 (ref. 52)
3	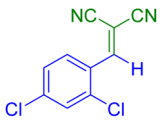 **3c**	15	95	126.6	506.4	148–150 (ref. 52)
4	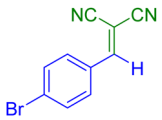 **3d**	17	92	122.6	437.8	162–164 (ref. 52)
5	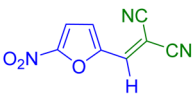 **3e**	10	93	124	775	180–182 (ref. 52)
6	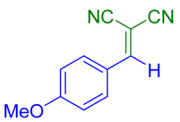 **3f**	40	89	118.6	179.7	111–113 (ref. 52)
7	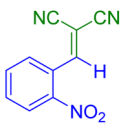 **3g**	10	92	122.6	766.6	138–140 (ref. 52)
8	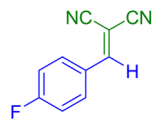 **3h**	15	89	118.6	474.6	125–127 (ref. 52)
9	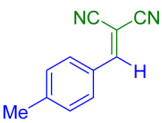 **3i**	40	88	117.3	177.7	132–134 (ref. 52)
10	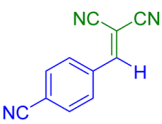 **3j**	8	96	128	984.6	154–156 (ref. 52)

Table 7 (*Contd.*)

Entry	Product	Time (min)	Yield[b] (%)	TON	TOF (h^{-1})	Reference
11	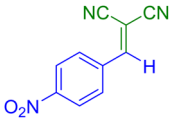 **3k**	8	95	126.6	974.3	160–162 (ref. 52)
12	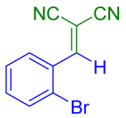 **3l**	17	91	121.3	433.2	91–93 (ref. 52)
13	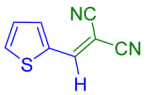 **3m**	20	90	120	363.3	100–102 (ref. 52)

[a] A mixture of various aldehyde (1 mmol) and malononitrile (1 mmol), catalyst (0.05 g, 0.75 mol%) in distilled water (2 mL) at room temperature was stirred. [b] Isolated pure yield.

the best result was obtained when the reaction was achieved using 0.05 g of the catalyst with the presence of distilled water at room temperature within 20 min with an efficiency of 95% (Table 6, entry 5). It was observed that by increasing the amount of catalyst from 0.07 to 0.1 g, no improvement was observed (Table 6, entries 6–8). The reaction was performed in the presence of other solvents, giving low yields of **3b** (Table 6, entries 9–14). When the reaction mixture was stirred at a temperature of 100 °C, it was noticed that the yield decreased (Table 6, entry 15).

After obtaining the optimal conditions, different derivatives of 2-benzylidenemalononitrile derivatives were synthesized using 0.05 g of the nanocatalyst, the results of which are presented in Table 7. As can be seen, from the reaction between different aldehydes with malononitrile, the desired products were obtained with an excellent yield of 88–96% after 8–40 min.

We also studied the gram scale synthesis on the reaction of 4-chlorobenzaldehyde, malononitrile and dimedone for the synthesis of derivative **4b** and the reaction of 4-chlorobenzaldehyde with malononitrile for the synthesis of derivative **3b** to demonstrate the ability of current method (Scheme 4). As can be seen, by stirring a mixture of 4-chlorobenzaldehyde (10 mmol), malononitrile (10 mmol) and dimedone (10 mmol) in EtOH (20 mL) and 4-chlorobenzaldehyde (10 mmol), malononitrile (10 mmol) in water (20 mL) at room temperature in the presence of catalyst, **4b** and **3b** can be synthesized with 88% and 89% yield, respectively.

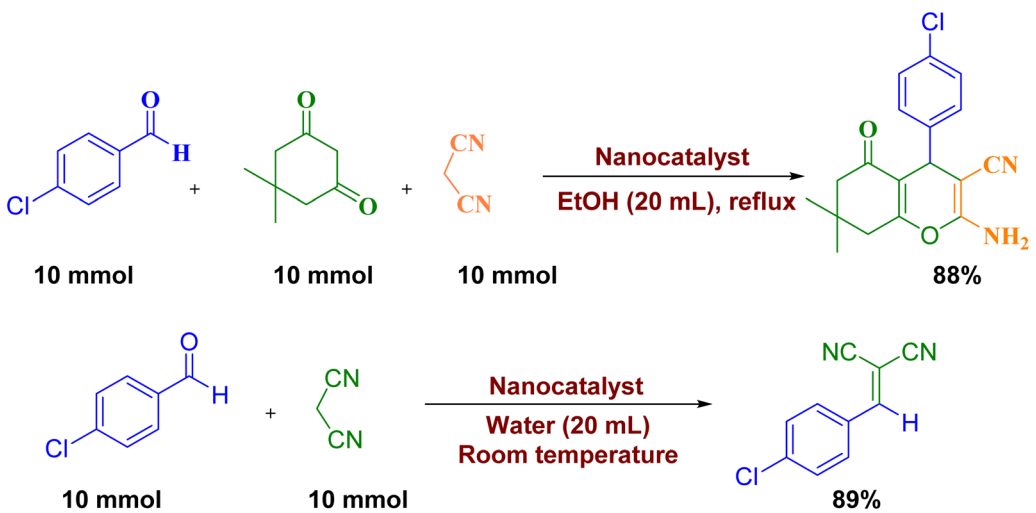

Scheme 4 Gram scale synthesis of **4b** and **3b**.

One of the important factors in the design of environmentally friendly nanocatalysis systems is the ability to recycle and reuse the catalyst. In order to investigate the recyclability and reusability of Cu(II)-Schiff-base-$(CH_2)_3$@SiO_2@Fe_3O_4, the reaction of 4-chlorobenzaldehyde, malononitrile and dimedone for the synthesis of derivative **4b** and the reaction of 4-chlorobenzaldehyde with malononitrile for the synthesis of derivative **3b** was selected as the model reaction under optimal conditions. After the completion of the reaction, the reaction mixture was cooled to room temperature. Then, the nanocatalyst was separated from the reaction mixture by an external field, washed with a mixture of water and ethanol, dried in air, and used to perform the reaction again. To check its catalytic power, the reaction was repeated seven times in the vicinity of this catalyst, and after seven times, the reaction efficiency decreased to 96 to 90% for **3b** and the reaction efficiency decreased to 96 to 91% for **4b**, respectively (Fig. 9a). The surface morphology of recycled sample after recycling seven times were conducted by TEM analysis (Fig. 9b). As shown in Fig. 9b, after recycling seven times, the surface morphology of recycled sample had not changed and stable against repeated use. Furthermore, the leaching experiment for the synthesis of **4b** after recycling over seven successive runs by ICP analysis was studied. The obtained results indicated that leaching of Cu is was very insignificant about 1.1%.

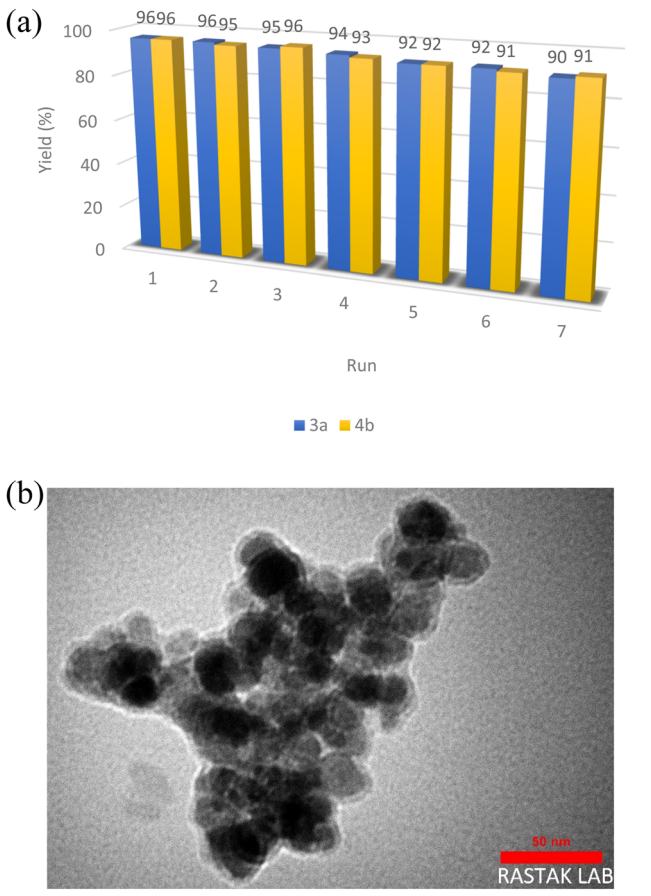

Fig. 9 (a) Reusability of as-prepared nanocatalyst during the model reaction and (b) TEM image of as-prepared nanocatalyst after seven times reuse.

Conclusion

In summary, we unveiled from the a novel heterogeneous magnetic nanocatalyst with core–shell morphology. The catalyst is easily synthesized *via* benign conditions and inexpensive precursors. Afterwards, the structural and magnetic characteristics of the produced nanoparticles were determined by employing using FT-IR, ICP, VSM, FE-SEM, TEM, TGA, PXRD, BET and EDX analyses. The performance of synthesized Cu(II)-Schiff-base-$(CH_2)_3$@SiO_2@Fe_3O_4 magnetic nanocatalyst has been tested for the 2-amino-4*H*-pyrans derivatives and 2-benzylidenemalononitrile derivatives. By evaluating the outcomes of different catalytic activity tests such as substrate scope analysis, leaching examination, recyclability tests, and gram scale experiments, one can ascertain the effectiveness of the synthesized Cu(II)-Schiff-base-$(CH_2)_3$@SiO_2@Fe_3O_4 catalyst. The advantages of these methods include easy separation and ability to recycle the catalyst after several times with high activity, use of solvent-free or green solvent conditions, use of available materials, no use of column chromatography, performing the reaction on a hot scale, short reaction time, production of products in high yield pointed out.

Author contributions

S. Rezayati and A. Ramazani conceived the idea and designed the research. M. Karimi carried out the research. M. Karimi wrote the original draft. S. Rezayati and A. Ramazani reviewed the manuscript and editing. A. Ramazani was responsible for the funding acquisition.

Conflicts of interest

There are no conflicts to declare.

Acknowledgements

The present study, derived from PhD thesis by Masoud Karimi, was supported by the Iran National Science Foundation INSF and the University of Zanjan.

References

1 S. K. Panja, N. Dwivedi and S. Saha, *RSC Adv.*, 2015, **5**, 65526–65531.
2 A. F. Trindade, P. M. Gois and C. A. Afonso, *Chem. Rev.*, 2009, **109**, 418–514.
3 A. Rai and K. V. Ranganath, *J. Heterocycl. Chem.*, 2021, **58**, 1039–1057.
4 Y. P. Yew, K. Shameli, M. Miyake, N. B. B. A. Khairudin, S. E. B. Mohamad, T. Naiki and K. X. Lee, *Arabian J. Chem.*, 2020, **13**, 2287–2308.
5 (*a*) E. A. Campos, D. V. B. S. Pinto, J. I. S. D. Oliveira, E. D. C. Mattos and R. D. C. L. Dutra, *J. Aerosp. Technol.*

Manage., 2015, **7**, 267–276; (*b*) F. Sheikholeslami-Farahani, *Asian J. Nanosci. Mater.*, 2022, **5**, 132–143; (*c*) S. Tabar Maleki and S. J. Sadati, *Asian J. Nanosci. Mater.*, 2022, **5**, 98–108.

6 (*a*) H. Pourfaraj, S. Rostamzadeh Mansour, M. Zaeifizadeh and A. Vojood, *Asian J. Nanosci. Mater.*, 2023, **6**, 92–105; (*b*) R. Khazaei, A. Khazaei and M. Nasrollahzadeh, *Appl. Organomet. Chem.*, 2023, **3**, 123–133; (*c*) N. Pourbahar and S. Sattari Alamdar, *Asian J. Green Chem.*, 2023, **7**, 9–16.

7 (*a*) H. Ghafuri, M. Zargari and A. Emami, *Asian J. Green Chem.*, 2023, **7**, 54–69; (*b*) F. Hakimi, A. Sharifi-Zarchi and E. Golrasan, *Chem. Methodol.*, 2023, **7**, 489–498; (*c*) E. Ezzatzadeh, *Asian J. Nanosci. Mater.*, 2021, **4**, 125–136; (*d*) M. B. Swami, G. R. Nagargoje, S. R. Mathapati, A. S. Bondge, A. H. Jadhav, S. P. Panchgalle and V. S. More, *Appl. Organomet. Chem.*, 2023, **3**, 184–198; (*e*) K. Yadollahzadeh, *Asian J. Nanosci. Mater.*, 2021, **4**, 81–94; (*f*) F. Hakimi, M. Taghvaee and E. Golrasan, *Adv. J. Chem., Sect. A*, 2023, **6**, 188–197.

8 Y. Zhao, Q. Zumin and J. Huang, *Chin. J. Chem. Eng.*, 2008, **16**, 451–455.

9 M. B. Gawande, P. S. Branco and R. S. Varma, *Chem. Soc. Rev.*, 2013, **42**, 3371–3393.

10 M. Bustamante-Torres, D. Romero-Fierro, J. Estrella-Nuñez, B. Arcentales-Vera, E. Chichande-Proaño and E. Bucio, *Polymers*, 2022, **14**, 752.

11 (*a*) B. H. Rotstein, S. Zaretsky, V. Rai and A. K. Yudin, *Chem. Rev.*, 2014, **114**, 8323–8359; (*b*) R. Muslim Muhiebes, L. Fatolahi and S. Sajjadifar, *Asian J. Green Chem.*, 2023, **7**, 121–131; (*c*) A. R. Moosavi-Zare, H. Goudarziafshar, Z. Jalilian and F. Hosseinabadi, *Chem. Methodol.*, 2022, **6**, 571–581; (*d*) S. Mowlazadeh Haghighi, A. Purkhosrow, A. Khalafi-Nezhad and S. Oftadehgan, *Asian J. Green Chem.*, 2022, **6**, 203–222; (*e*) S. Dey, P. Basak, S. Sarkar and P. Ghosh, *Asian J. Green Chem.*, 2022, **6**, 24–39.

12 T. Zarganes-Tzitzikas, A. L. Chandgude and A. Dömling, *Chem. Rec.*, 2015, **15**, 981–996.

13 J. E. Biggs-Houck, A. Younai and J. T. Shaw, *Curr. Opin. Chem. Biol.*, 2010, **14**, 371–382.

14 G. Bosica and R. Abdilla, *Catalysts*, 2022, **12**, 725.

15 R. H. Vekariya and H. D. Patel, *Synth. Commun.*, 2014, **44**, 2756–2788.

16 A. Samui, N. Kesharwani, C. Haldar and S. K. Sahu, *Microporous Mesoporous Mater.*, 2020, **299**, 110112.

17 D. B. Shinde, S. Kandambeth, P. Pachfule, R. P. Kumar and R. Banerjee, *Chem. Commun.*, 2015, **51**, 310–313.

18 M. L. Gao, M. H. Qi, L. Liu and Z. B. Han, *Chem. Commun.*, 2019, **55**, 6377–6380.

19 Y. X. Ma, Z. J. Li, L. Wei, S. Y. Ding, Y. B. Zhang and W. Wang, *J. Am. Chem. Soc.*, 2017, **139**, 4995–4998.

20 C. Viel and J. C. Doré, *Farmaco Sci.*, 1972, **27**, 257–312.

21 A. Sidhu, J. R. Sharma and M. Rai, *Indian J. Chem., Sect. B: Org. Chem. Incl. Med. Chem.*, 2010, **49**, 247–250.

22 S. A. Khan, A. M. Asiri, R. M. Rahman, S. A. Elroby, F. M. S. Aqlan, M. Y. Wani and K. Sharma, *J. Heterocycl. Chem.*, 2017, **54**, 3099–3107.

23 A. S. Fouda, Y. A. El-Ewady, O. M. Abo-El-Enien and F. A. Agizah, *Anti-Corros. Methods Mater.*, 2008, **55**, 317–323.

24 H. Jin, M. Liang, S. Arzhantsev, X. Li and M. Maroncelli, *J. Phys. Chem. B*, 2010, **114**, 7565–7578.

25 Z. Tashrifi, M. Mohammadi-Khanaposhtani, H. Hamedifar, B. Larijani, S. Ansari and M. Mahdavi, *Mol. Diversity*, 2020, **24**, 1385–1431.

26 S. Saneinezhad, L. Mohammadi, V. Zadsirjan, F. F. Bamoharram and M. M. Heravi, *Sci. Rep.*, 2020, **10**, 1–26.

27 H. Kiyani and F. Ghorbani, *Chem. Pap.*, 2014, **68**, 1104–1112.

28 M. Aghajani, S. Asghari, G. F. Pasha and M. Mohseni, *Res. Chem. Intermed.*, 2020, **46**, 1841–1855.

29 E. Kolvari, N. Koukabi, Z. Ozmaei, H. Khoshkho and F. Seidi, *Curr. Res. Green Sustainable Chem.*, 2022, **5**, 100327.

30 J. Safaei-Ghomi, A. Javidan, A. Ziarati and H. Shahbazi-Alavi, *J. Nanopart. Res.*, 2015, **17**, 1–12.

31 F. Mohammadpour, *Polycyclic Aromat. Compd.*, 2021, **41**, 160–172.

32 M. Lashkari, F. Mohamadpour, M. T. Maghsoodlou, R. Heydari and N. Hazeri, *Polycyclic Aromat. Compd.*, 2020, **56**, 1123–1134.

33 B. Sunil Kumar, N. Srinivasulu, R. H. Udupi, B. Rajitha, Y. Thirupathi Reddy, P. Narsimha Reddy and P. S. Kumar, *J. Heterocycl. Chem.*, 2006, **43**, 1691–1693.

34 P. Singh, P. Yadav, A. Mishra and S. K. Awasthi, *ACS Omega*, 2020, **5**, 4223–4232.

35 A. Maleki and Z. Hajizadeh, *Silicon*, 2019, **11**, 2789–2798.

36 H. Ebrahimiasl and D. Azarifar, *Appl. Organomet. Chem.*, 2020, **34**, e5359.

37 Z. J. Yang, Q. T. Gong, Y. Wang, Y. Yu, Y. H. Liu, N. Wang and X. Q. Yu, *Mol. Catal.*, 2020, **491**, 456–470.

38 Saigal, M. Irfan, P. Khan, M. Abid and M. M. Khan, *ACS Omega*, 2019, **4**, 16794–16807.

39 R. Muslim Mhaibes, Z. Arzehgar, M. Mirzaei Heydari and L. Fatolahi, *Asian J. Green Chem.*, 2023, **7**, 1–8.

40 B. Baghernejad and S. M. Hojati, *Asian J. Green Chem.*, 2022, **6**, 194–202.

41 K. Yadollahzadeh, *Asian J. Nanosci. Mater.*, 2022, **5**, 144–158.

42 H. Taherkhani, A. Ramazani, S. Sajjadifar, H. Aghahosseini, A. Rezaei and S. Rezayati, *ChemistrySelect*, 2021, **6**, 1–14.

43 S. Rezayati, G. Dinmohammadi, A. Ramazani and S. Sajjadifar, *Polycyclic Aromat. Compd.*, 2023, **43**, 5869–5891.

44 P. Singh, P. Yadav, A. Mishra and S. K. Awasthi, *ACS Omega*, 2020, **5**, 4223–4232.

45 G. Rathee, S. Kohli, S. Panchal, N. Singh, A. Awasthi, S. Singh, A. Singh, S. Hooda and R. Chandra, *ACS Omega*, 2020, **5**, 23967–23974.

46 E. Pourian, S. Javanshir, Z. Dolatkhah, S. Molaei and A. Maleki, *ACS Omega*, 2018, **3**, 5012–5020.

47 (*a*) S. Rezayati, F. Kalantari and A. Ramazani, *RSC Adv.*, 2023, **13**, 12869; (*b*) F. Kalantari, S. Rezayati and A. Ramazani., *Appl. Organomet. Chem.*, 2023, **37**, e7064; (*c*) G. Mansouri, M. Abdizad, A. R. Abbasi and S. Rezayati, *Appl. Organomet. Chem.*, 2022, **36**, e6866; (*d*) S. Rezayati, H. Haghighat and A. Ramazani, *Silicon*, 2023, **15**, 2679–2692; (*e*) S. Rezayati, Y. Ahmadi and A. Ramazani, *Inorg. Chim. Acta*, 2023, **544**,

121203; (*f*) S. Rezayati, Z. Naserifar and A. Ramazani, *Phosphorus, Sulfur Silicon Relat. Elem.*, 2022, **197**, 1016–1025; (*g*) S. Rezayati, F. Kalantari, A. Ramazani and E. Ezzatzadeh, *J. Sulfur Chem.*, 2021, **42**, 575–590; (*h*) S. Rezayati, R. Hajinasiri and Z. Erfani, *Res. Chem. Intermed.*, 2016, **42**, 2567–2576; (*i*) S. Rezayati, M. Mehmannavaz, E. Salehi, Sh. Haghi, R. Hajinasiri and S. Afshari Sharif Abad, *J. Sci., Islamic Repub. Iran*, 2016, **27**, 51–63; (*j*) S. Rezayati, E. Rezaee Nezhad and R. Hajinasiri, *Chin. Chem. Lett.*, 2016, **27**, 974–978; (*k*) S. Rezayati and S. Sajjadifar, *J. Sci., Islamic Repub. Iran*, 2014, **25**, 329–337.

48 S. Rezayati, A. Ramazani, S. Sajjadifar, H. Aghahosseini and A. Rezaei, *ACS Omega*, 2021, **6**, 25608–25622.

49 M. Mirzaee, B. Bahramian, P. Gholampour, T. Teymouri and T. Khorsand, *Appl. Organomet. Chem.*, 2019, **33**, e4792.

50 F. Kalantari, A. Ramazani, M. R. Poor Heravi, H. Aghahosseini and K. Ślepokura, *Inorg. Chem.*, 2021, **60**, 15010–15023.

51 S. Amirnejat, A. Nosrati, R. Peymanfar and S. Javanshir, *Res. Chem. Intermed.*, 2020, **46**, 3683–3701.

52 F. Kalantari, S. Rezayati, A. Ramazani, H. Aghahosseini, K. Ślepokura and T. Lis, *ACS Appl. Nano Mater.*, 2022, **5**, 1783–1797.